



HAL
open science

Nuclear spin conservation enables state-to-state control of ultracold molecular reactions

Ming-Guang Hu, Yu Liu, Matthew A. Nichols, Lingbang Zhu, Goulven Quéméner, Olivier Dulieu, Kang-Kuen Ni

► **To cite this version:**

Ming-Guang Hu, Yu Liu, Matthew A. Nichols, Lingbang Zhu, Goulven Quéméner, et al.. Nuclear spin conservation enables state-to-state control of ultracold molecular reactions. *Nature Chemistry*, 2021, 13, pp.435-440. 10.1038/s41557-020-00610-0 . hal-02619604

HAL Id: hal-02619604

<https://hal.science/hal-02619604>

Submitted on 7 Dec 2021

HAL is a multi-disciplinary open access archive for the deposit and dissemination of scientific research documents, whether they are published or not. The documents may come from teaching and research institutions in France or abroad, or from public or private research centers.

L'archive ouverte pluridisciplinaire **HAL**, est destinée au dépôt et à la diffusion de documents scientifiques de niveau recherche, publiés ou non, émanant des établissements d'enseignement et de recherche français ou étrangers, des laboratoires publics ou privés.

Nuclear spin conservation enables state-to-state control of ultracold molecular reactions

Ming-Guang Hu,^{1,2,3,*} Yu Liu,^{2,1,3,*} Matthew A. Nichols,^{1,2,3}
Lingbang Zhu,^{1,2,3} Goulven Quémener,⁴ Olivier Dulieu,⁴ and Kang-Kuen Ni^{1,2,3,†}

¹*Department of Chemistry and Chemical Biology,
Harvard University, Cambridge, Massachusetts, 02138, USA.*

²*Department of Physics, Harvard University, Cambridge, Massachusetts, 02138, USA.*

³*Harvard-MIT Center for Ultracold Atoms, Cambridge, Massachusetts, 02138, USA.*

⁴*Université Paris-Saclay, CNRS, Laboratoire Aimé Cotton, 91405, Orsay, France*

(Dated: December 6, 2021)

Quantum control of reactive systems has enabled microscopic probes of underlying interaction potentials, the opening of novel reaction pathways, and the alteration of reaction rates using quantum statistics. However, extending such control to the quantum states of reaction outcomes remains challenging. In this work, we realize this goal through the nuclear spin degree of freedom, a result which relies on the conservation of nuclear spins throughout the reaction. Using resonance-enhanced multiphoton ionization spectroscopy to investigate the products formed in bimolecular reactions between ultracold KRb molecules, we find that the system retains a near-perfect memory of the reactants nuclear spins, manifested as a strong parity preference for the rotational states of the products. We leverage this effect to alter the occupation of these product states by changing the superposition of initial nuclear spin states with an external magnetic field. The techniques demonstrated here open up the possibility to study ultracold reaction dynamics at the state-to-state level as well as quantum entanglement between reaction products.

* These authors contributed equally.

† To whom correspondence should be addressed. E-mail: ni@chemistry.harvard.edu

Controlling reactions between molecules at the level of individual quantum states is a long-standing goal in chemistry and physics [1]. Recent advancements in cold and ultracold techniques granted control over all molecular degrees of freedom, including electronic, rotation, vibration, nuclear spin, and partial waves of scattering [2, 3]. This has enabled the understanding and manipulation of chemical reactions free from thermal ensemble averaging [4–6]. In particular, the preparation of cold reactants in single quantum states has facilitated studies of scattering resonances which probe interaction potentials with exceptional resolution [7–10], efficient steering of reactive pathways to form selected product species [11, 12], and modification of long-range interactions to dramatically alter the overall rates of reactions [13–17]. While these results have improved our fundamental understanding of chemical processes, gaining control over the quantum states in which reaction products are formed is a next milestone [18]. Despite much experimental effort, the ability to detect, let alone exert control over, the quantum states of product species in these cold and ultracold reactions has remained challenging.

A fundamental factor standing in the way of product control in low-temperature reactions is the fact that they are typically barrierless, and proceed through the formation of intermediate complexes [19], which can live for a duration significantly longer than the characteristic rovibrational timescale of the system. As a result, the energy of the complex is expected to be well-mixed into its various degrees of freedom, leading to a statistical distribution of the reaction products in which the effect of the reactant state preparation is strongly suppressed [20]. One notable exception to this behavior, however, is that spins of the nuclei involved tend to remain unchanged throughout reactions [21, 22]. This phenomenon has been observed in both complex-forming [23–25] and direct [26] bimolecular reactions, as well as in photodissociations [27–29], and was attributed to weak coupling between nuclear spins and other degrees of freedom. As such, nuclear spins provide a promising handle via which control over ultracold reactions can be exerted.

Previous studies on the behavior of nuclear spins have focused on reactions involving hydrogen-containing species, due largely to their relevance in astrochemical processes. The results of these studies helped establish the well-accepted rule of nuclear spin conservation in chemical reactions [22]. Ultracold reactions, on the other hand, display unique characteristics that may challenge the robustness of this rule. Specifically, nuclei involved in these reactions can possess spins many times higher than those found in prior works, which were protons with spin of $1/2$. This can result in stronger couplings between the spins and other

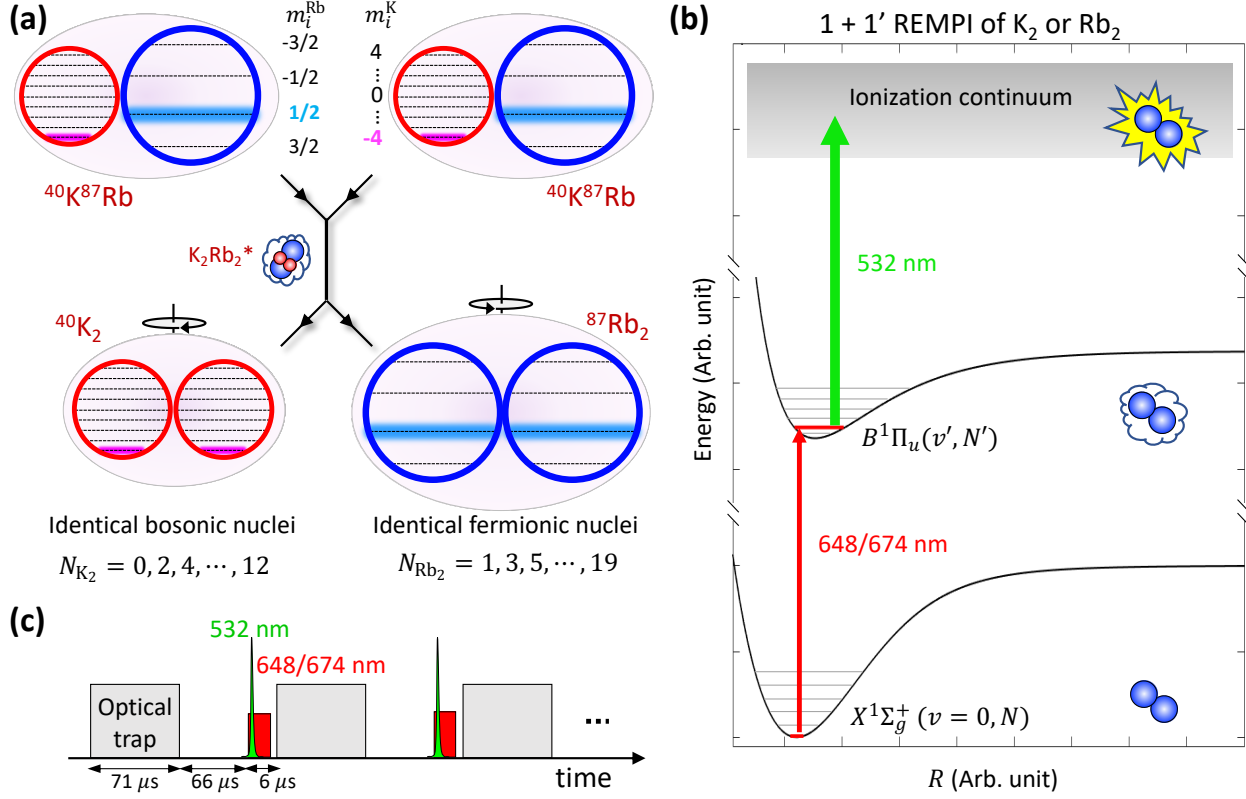


FIG. 1. **Testing the conservation of nuclear spins in bimolecular reactions between ultracold KRb molecules using REMPI spectroscopy.** (a) Schematic illustration of the conservation of nuclear spin throughout the reaction $\text{KRb} + \text{KRb} \rightarrow \text{K}_2\text{Rb}_2^* \rightarrow \text{K}_2 + \text{Rb}_2$ at $B = 30$ G. In this case, the initial reactant nuclear spin states $m_i^K = -4$ and $m_i^{\text{Rb}} = 1/2$ are inherited by the product nuclei, resulting in symmetric product nuclear spin states. Due to the exchange symmetry of the identical bosonic (fermionic) nuclei of K_2 (Rb_2), their rotational states are restricted to even (odd) parity. (b) The REMPI scheme used to identify rovibrational states of products. K_2 and Rb_2 molecules are state-selectively photoionized from the initial quantum state, $X^1\Sigma_g^+(v=0, N)$, via an intermediate state, $B^1\Pi_u(v', N')$. Here, v and v' are vibrational quantum numbers; N and N' are rotational quantum numbers. (c) Timing diagram for product ionization and detection. The optical trap confining the reactant KRb molecules is square-wave modulated at 7 kHz. During the dark phase of the modulation, K_2 and Rb_2 products are generated by the reaction, ionized using REMPI, and detected by ion mass spectrometry. The sequence is repeated for a duration of 1 s, until all reactants in the trap are depleted.

degrees of freedom. Furthermore, the intermediate complex involved in these reactions can be exceptionally long-lived [30, 31], which provides more time for these couplings to alter the spins. Thus, the behavior of nuclear spins in ultracold reactions is an open question and remains to be experimentally examined. In prior studies, such examinations were carried out in systems involving cascaded reactions, using reactants with statistically mixed nuclear spins. Ultracold molecules, in contrast, can be prepared in single nuclear spin states, and react via single collisions. Hence, they provide a unique platform to cleanly test the

conservation of nuclear spins.

In this study, we show that nuclear spins are conserved throughout the ultracold reaction $^{40}\text{K}^{87}\text{Rb} + ^{40}\text{K}^{87}\text{Rb} \rightarrow \text{K}_2\text{Rb}_2^* \rightarrow ^{40}\text{K}_2 + ^{87}\text{Rb}_2$ (Fig. 1(a)), where the K and Rb nuclei have high nuclear spins of 4 and 3/2, respectively, and the intermediate complex K_2Rb_2^* has a long lifetime of 360(30) ns [32]. Because the products are homonuclear diatomic molecules, by the exchange symmetry of identical particles, their rotational states are correlated to their nuclear spin states [33]. Using resonance-enhanced multiphoton ionization (REMPI) spectroscopy to probe the rotational states of the products, we find K_2 molecules predominantly in even-parity rotational states ($N_{\text{K}_2} = 0, 2, \dots, 12$) and Rb_2 in odd ($N_{\text{Rb}_2} = 1, 3, \dots, 19$), consistent with nuclear spin conservation. Utilizing this conservation, we demonstrate a technique to continuously alter the state distributions of the products by changing the superposition state of the reactant nuclear spins with an applied magnetic field. We model this behavior as a projection of the spin state of the reactant nuclei onto the symmetric or antisymmetric spin states of the product nuclei.

Our experiment begins with a trapped gas of $X^1\Sigma^+(v = 0, N_{\text{KRb}} = 0)$ ground-state KRb molecules prepared in a single hyperfine state. Here v and N are vibrational and rotational quantum numbers, respectively. In each experimental cycle, we typically prepare 10^4 molecules in a crossed optical dipole trap with a temperature of 500 nK and a peak density of 10^{12} cm^{-3} . Details of the apparatus regarding the production and detection of the gas were reported elsewhere [34]. In the presence of a sufficiently large magnetic bias field ($B > 20$ G), the spins of the K and Rb nuclei are decoupled from one another, and the hyperfine state of the molecules can be written as $|i_{\text{K}} = 4, i_{\text{Rb}} = 3/2, m_i^{\text{K}} = -4, m_i^{\text{Rb}} = 1/2\rangle$, where i and m_i are the nuclear spins and their projections along the bias field, respectively [35, 36]. Once prepared, the molecules undergo the exchange reaction



for which the product species were previously confirmed by combining single-photon ionization and ion mass spectrometry [37]. Here, using state-controlled reactants at $B = 30$ G, we investigate the conservation of nuclear spins throughout this reaction.

While directly probing the nuclear spin states of products is challenging due to their small energy splitting, we can infer this information from the parity of their rotational states. For homonuclear diatomic molecules such as K_2 and Rb_2 , nuclear spin and rotation are linked by the exchange symmetry of identical particles [33]. In $^{40}\text{K}_2$, where the nuclei are bosonic, spin states that are symmetric under the exchange of nuclei require rotational states

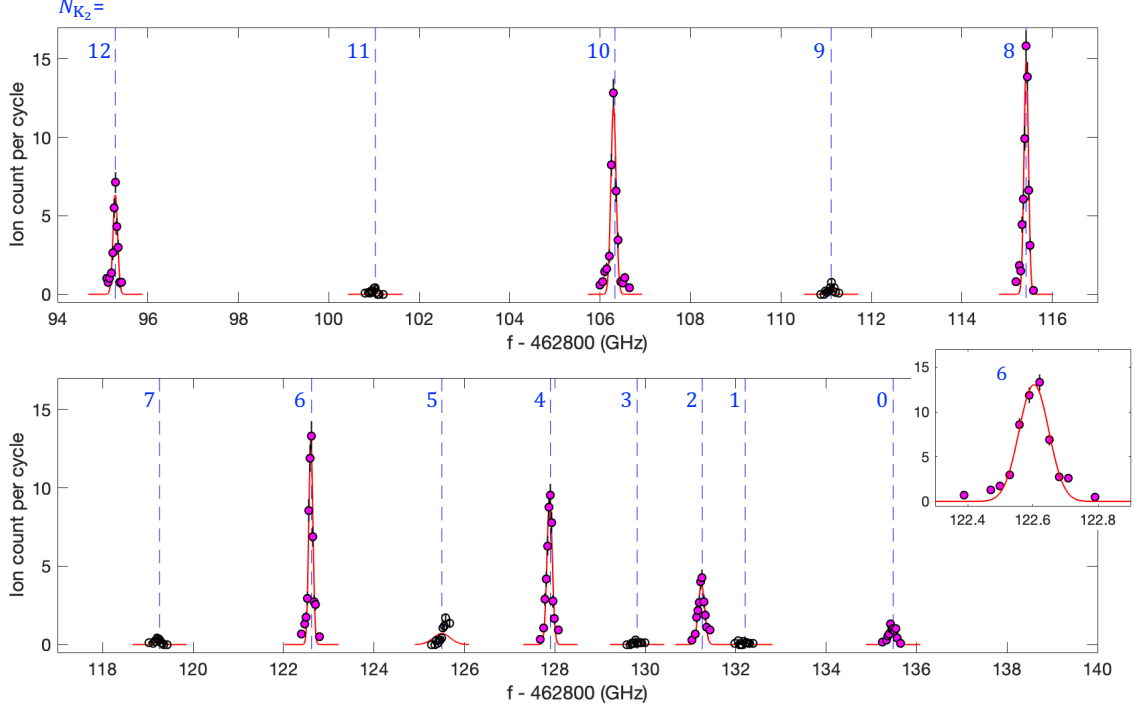


FIG. 2. **REMPI spectrum for $^{40}\text{K}_2$ product molecules.** By scanning the 648 nm laser frequency to search for rotational lines within the $X^1\Sigma_g^+(v=0, N_{\text{K}_2}) \rightarrow B^1\Pi_u(v'=1, N'_{\text{K}_2})$ vibronic band, we observe strong K_2^+ signals at frequencies corresponding to rotational states with even values of N_{K_2} , and highly suppressed signals for odd values. The ion count for each data point is normalized by the corresponding number of experimental cycles (~ 16); the error bars denote shot noise. For $N_{\text{K}_2} > 0$ we drive transitions with $N'_{\text{K}_2} - N_{\text{K}_2} = 0$ (Q branch), whereas for $N_{\text{K}_2} = 0$, we drive the only allowed transition, with $N'_{\text{K}_2} - N_{\text{K}_2} = 1$ (R branch). Blue dashed lines indicate the predicted transition frequencies. The relatively strong asymmetric signal associated with $N_{\text{K}_2} = 5$ is due to a nearby $N_{\text{K}_2} = 2 \rightarrow N'_{\text{K}_2} = 1$ (P branch) transition at 462925.68 GHz. We do not observe any signals at frequencies corresponding to states with $N_{\text{K}_2} > 12$. Gaussian fits (red curves) are applied to each signal peak, yielding a typical spectral linewidth (1σ) of ~ 50 MHz. (Inset) Lineshape for the transition $N_{\text{K}_2} = 6 \rightarrow N'_{\text{K}_2} = 6$; the Gaussian width is $\sigma = 46 \pm 4$ MHz.

with even parity, while those that are antisymmetric require odd parity. In $^{87}\text{Rb}_2$, where the nuclei are fermionic, this symmetry-parity correspondence is switched. Therefore, if nuclear spins are conserved over the reaction, K_2 and Rb_2 will have symmetric spin states $|i_{\text{K}} = 4, i_{\text{K}} = 4, m_i^{\text{K}} = -4, m_i^{\text{K}} = -4\rangle$ and $|i_{\text{Rb}} = 3/2, i_{\text{Rb}} = 3/2, m_i^{\text{Rb}} = 1/2, m_i^{\text{Rb}} = 1/2\rangle$, respectively, allowing only even rotational states of K_2 and odd rotational states of Rb_2 to be occupied. This outcome is easily distinguishable from that where the nuclear spin states are statistically occupied. In this case, the population ratio between even and odd rotational states would be 5/4 for K_2 and 3/5 for Rb_2 , as determined by the numbers of symmetric and antisymmetric spin states in each molecule [33].

To detect the product rotational states, we use a $1 + 1'$ REMPI technique, which con-

sists of an initial single-photon bound-to-bound transition from the electronic and vibrational ground-state $X^1\Sigma_g^+(v = 0, N)$ to an electronically excited intermediate-state $B^1\Pi_u(v', N')$, followed by a single-photon bound-to-continuum transition that ionizes the molecules (Fig. 1(b)). We drive the bound-to-bound transition using a frequency-tunable laser operating around 648 nm for the detection of K_2 and 674 nm for Rb_2 . The bound-to-continuum transition is excited by a 532 nm pulsed laser for both product species. Figure 1(c) shows the timing diagram for product ionization and detection. Because the trap light can alter the outcome of the reaction [32], we apply a 7 kHz square wave modulation to its intensity, and probe the products during the dark phases of the modulation using REMPI pulses and ion mass spectrometry. In each cycle, ion signals are recorded until all the KRb reactants in the sample are depleted (~ 1 s). To avoid photoexcitation of the KRb molecules by the REMPI lasers [38, 39], we shape the beams to have dark spots centered on the trapped sample (Fig. S1). Products, on the other hand, escape the trap because of their significant translational energies, and a reasonable portion ($\sim 30\%$) of them are illuminated by the REMPI beams before they leave the detection region.

To identify the occupied rotational states of the products, we scan the 648/674 nm laser frequency to search for resonances around the $\Delta N = N' - N = 0$ (Q branch) transitions, and compare our measurements with theoretical calculations based on molecular potentials fitted by prior spectroscopic data [40–44]. The results are shown in Fig. 2 for K_2 and Fig. 3 for Rb_2 . We observe resonant signals corresponding to the states $N = 0 - 12$ for K_2 and $0 - 19$ for Rb_2 , at frequencies that match the predicted values to within our measurement precision. The spectral widths of these resonances (insets) arise from the natural linewidth, the laser frequency uncertainty, and the Doppler width (see SM). We also search for states beyond $N_{K_2} = 12$ and $N_{Rb_2} = 19$, which are energetically forbidden based on the calculated reaction exothermicity of 9.54 cm^{-1} [45], and find their populations to be consistent with zero. Among those that are energetically accessible, we find populations predominantly in the even states of K_2 and odd states of Rb_2 . This significantly deviates from statistical behavior, and provides direct evidence for the conservation of nuclear spins in a reaction involving high-spin nuclei and a long-lived intermediate complex. We note that the amplitudes of the resonances in Figs. 2 and 3 are not yet sufficient to directly reconstruct the intrinsic product state distribution governed by the reaction dynamics, due to uncertainties in the state-dependent ionization efficiencies.

Given the strong rotational parity preference exhibited by a simple hyperfine state of the

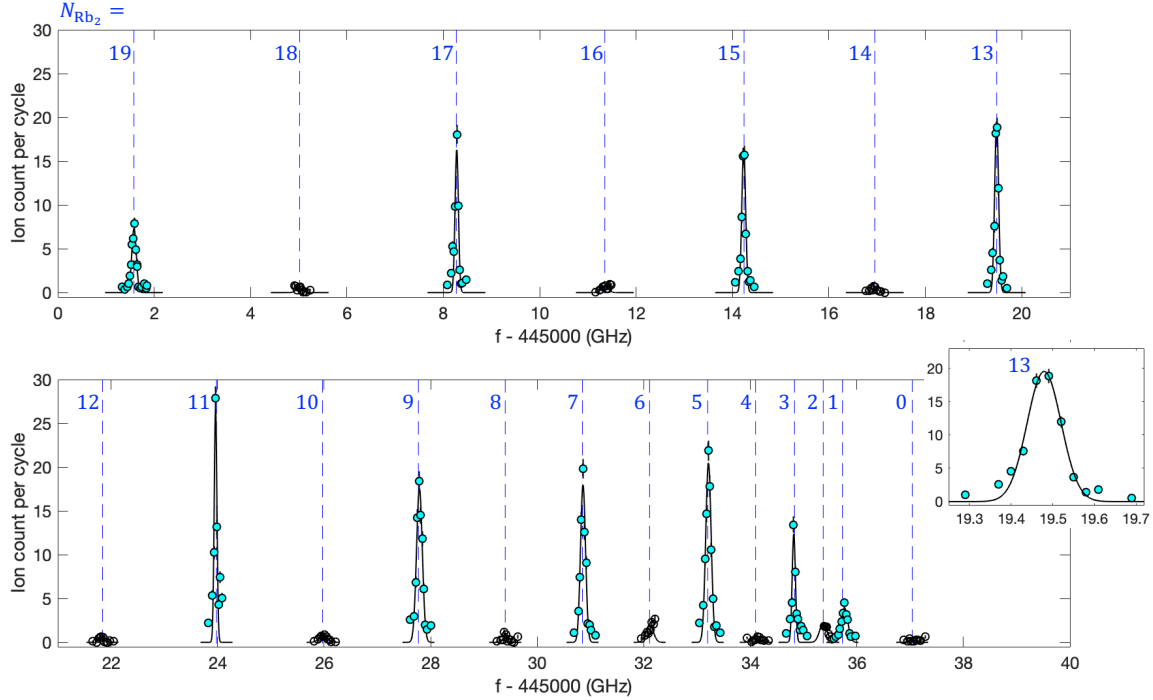


FIG. 3. **REMPI spectrum for $^{87}\text{Rb}_2$ product molecules.** The frequency of the 674 nm laser is scanned within the $X^1\Sigma_g^+(v=0, N_{\text{Rb}_2}) \rightarrow B^1\Pi_u(v'=4, N'_{\text{Rb}_2})$ vibronic band. We observe strong Rb_2^+ signals for transitions from odd rotational states, and highly suppressed signals from even ones. The ion count for each data point is normalized by the corresponding number of experimental cycles (~ 16); the error bars denote shot noise. We drive Q branch transitions for $N_{\text{Rb}_2} > 0$, and R branch for $N_{\text{Rb}_2} = 0$. Blue dashed lines indicate the predicted transition frequencies. The relatively strong asymmetric signal associated with $N_{\text{Rb}_2} = 6$ is due to a nearby $N_{\text{Rb}_2} = 15 \rightarrow N'_{\text{Rb}_2} = 16$ (R branch) transition at 445032.31 GHz, while that with $N_{\text{Rb}_2} = 2$ is due to a $N_{\text{Rb}_2} = 13 \rightarrow N'_{\text{Rb}_2} = 14$ (R branch) transition at 445035.30 GHz. We do not observe any signals at frequencies corresponding to states with $N_{\text{Rb}_2} > 19$. Gaussian fits (black curves) are applied to each signal peak, yielding a typical spectral linewidth (1σ) of ~ 40 MHz. (Inset) Lineshape for the transition $N_{\text{Rb}_2} = 13 \rightarrow N'_{\text{Rb}_2} = 13$; the Gaussian width is $\sigma = 43 \pm 3$ MHz.

reactants, one can consider how such conservation manifests itself for a more general form of the state. To explore this, we adjust the spin superposition of the KRb reactants by tuning the bias field. After initializing the molecules in the state $|4, 3/2, -4, 1/2\rangle$, we adiabatically ramp the field to a final value B , where the nuclear spin state of reactants takes the form,

$$\psi_{\text{KRb}} = \alpha \left| 4, \frac{3}{2}, -4, \frac{1}{2} \right\rangle + \beta \left| 4, \frac{3}{2}, -3, -\frac{1}{2} \right\rangle + \gamma \left| 4, \frac{3}{2}, -2, -\frac{3}{2} \right\rangle. \quad (2)$$

The admixture probabilities, $|\alpha|^2$, $|\beta|^2$, and $|\gamma|^2$, are calculated by diagonalizing the hyperfine Hamiltonian of KRb [35, 36] as a function of B , as shown in Fig. 4(a). For $B \gtrsim 20$ G, one has $|\alpha|^2 \approx 1$, and the reactant state is dominated by $|4, 3/2, -4, 1/2\rangle$. For $B \lesssim 20$ G, the state becomes significantly mixed with the other two spin components. With this form of the input state, we probe the outcome of the reaction for values of B in the range 5 – 50 G. Without

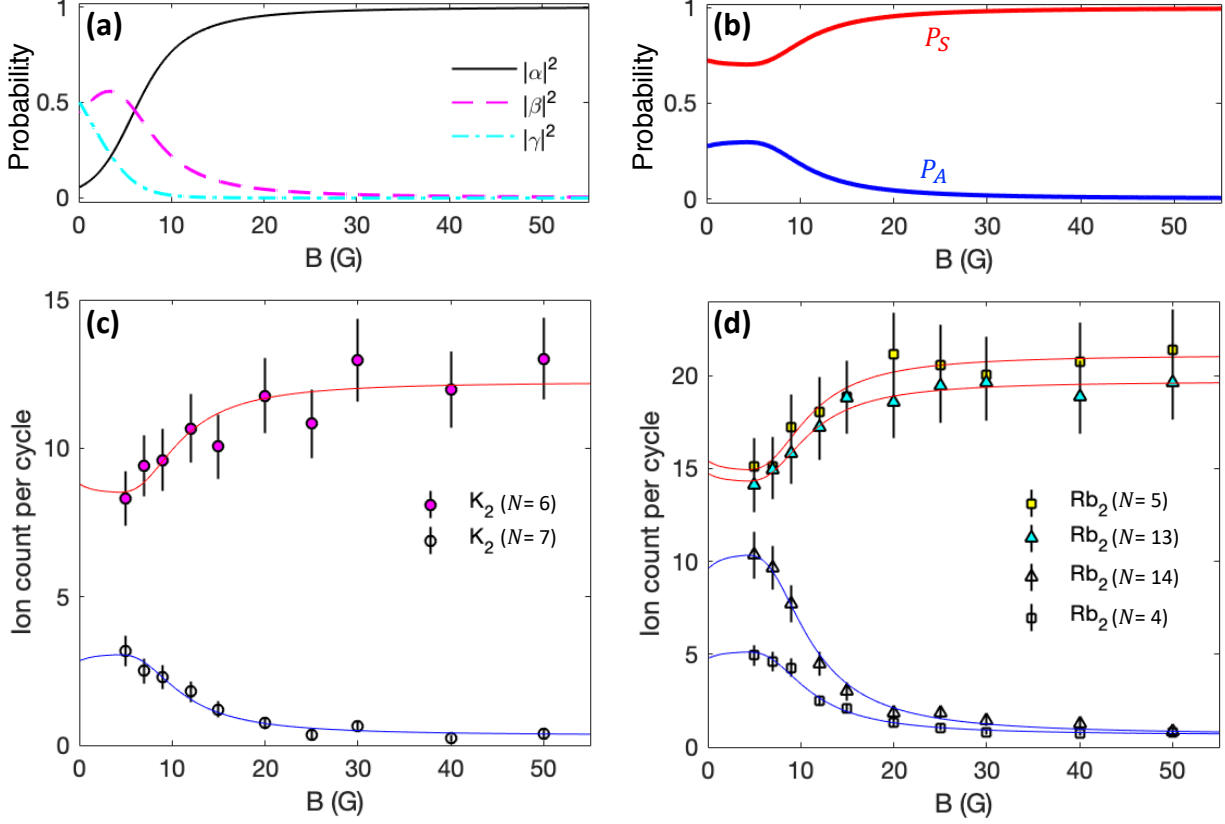


FIG. 4. **Controlling the occupation of product rotational states using an external magnetic field.** (a) Calculated admixture probabilities $|\alpha|^2$, $|\beta|^2$, and $|\gamma|^2$ for the reactant spin superposition (Eq. 2) as a function of magnetic field. (b) Probabilities for scattering into the symmetric (P_S) and antisymmetric (P_A) nuclear spin states of K_2 or Rb_2 based on the conservation of nuclear spins. (c,d) Product ion counts associated with the rotational states $N = 6, 7$ for K_2 (c) and $N = 4, 5, 13, 14$ for Rb_2 (d) obtained at different magnetic field values between 5 and 50 G. For each data set, the 648/674 nm laser frequency is fixed to be resonant with the corresponding transition, as identified from the spectra in Figs. 2 and 3. The ion count for each data point is normalized by the corresponding number of experimental cycles (~ 20). Error bars include shot noise and 10% ion number fluctuation due to the REMPI laser frequency uncertainty (~ 25 MHz). Red (blue) curves are fits to the function $a \cdot P_{S(A)} + b$, where a and b are fit parameters representing the state-dependent proportionality constant and the offset arising from the detection noise floor, respectively. The typical root-mean-square error (RMSE) for the fit is 0.35.

loss of generality, we measure changes in the amplitudes of the resonances corresponding to the rotational states $N = 6, 7$ for K_2 and $N = 4, 5, 13, 14$ for Rb_2 (Fig. 4(c,d)). We observe that the odd (even) states of K_2 (Rb_2), which are unoccupied at higher magnetic fields, acquire significant population as B decreases, while the population in the even (odd) states are suppressed. This result shows that the relative occupation of odd and even parity states of the products can be altered experimentally by controlling the nuclear spins of reactants via an external field.

We model this behavior using a selection rule based on angular momentum algebra, which is derived in accordance with the conservation of nuclear spins throughout the reaction (SM). Given the form of the reactant input state (Eq. 2), the probabilities for scattering into the antisymmetric (A) and symmetric (S) spin states of K_2 or Rb_2 are found to be $P_A = |\alpha\beta|^2 + |\alpha\gamma|^2 + |\beta\gamma|^2$ and $P_S = 1 - P_A$, respectively. The magnetic field dependence of these probabilities, shown in Fig. 4(b), derives from that of the admixture coefficients (Fig. 4(a)). Because of the exchange symmetry of identical nuclei, the detected populations of even (odd) rotational states are proportional to P_S (P_A) for K_2 and P_A (P_S) for Rb_2 . The constant of proportionality depends on the rotational state distribution resulting from the reaction dynamics, as well as the state-dependent ionization efficiency, and is therefore unique for each rotational state. As a result, we fit each data set in Fig. 4(c,d) to the function $a \cdot P_{S/A} + b$, with free parameters a and b . Here, a represents the aforementioned proportionality constant, and b is an offset arising from the noise floor of the detection. The fitted curves (Fig. 4(c,d)) show that our model for $P_{S/A}$ describes well the magnetic field dependence of the rotational state populations.

While this model was derived for a specific input state, Eq. (2), the methodology does not depend on the particular form of this state, and can be generalized to account for arbitrary states of the reactant nuclear spins. Experimentally, such states may be realized using a combination of external magnetic fields and microwave control techniques [35, 46–48]. With this capability, the product state control demonstrated here can be used to establish selected parity correlations between products originating from the same reaction. Such correlations will allow for the generation of quantum entanglement between reaction products [49, 50].

ACKNOWLEDGMENTS

We thank T. Rosenband for providing the code used to calculate the molecular hyperfine structure, J. Bohn for discussions, and R. Vexiau for calculations of relevant molecular transitions. **Funding:** This work is supported by the DOE Young Investigator Program, the David and Lucile Packard Foundation, and the NSF through the Harvard-MIT CUA. M.A.N. is supported by a HQI fellowship. G.Q. acknowledges funding from the FEW2MANY-SHIELD Project No. ANR-17-CE30-0015 from Agence Nationale de la Recherche.

[1] J. C. Polanyi, Accounts of Chemical Research **5**, 161 (1972).

- [2] G. Quemener and P. S. Julienne, *Chemical Reviews* **112**, 4949 (2012).
- [3] J. Jankunas and A. Osterwalder, *Annual Review of Physical Chemistry* **66**, 241 (2015).
- [4] R. V. Krems, *Physical Chemistry Chemical Physics* **10**, 4079 (2008).
- [5] N. Balakrishnan, *The Journal of Chemical Physics* **145**, 150901 (2016).
- [6] J. Toscano, H. Lewandowski, and B. R. Heazlewood, *Physical Chemistry Chemical Physics* **22**, 9180 (2020).
- [7] A. Klein, Y. Shagam, W. Skomorowski, P. S. Żuchowski, M. Pawlak, L. M. C. Janssen, N. Moiseyev, S. Y. van de Meerakker, A. van der Avoird, C. P. Koch, and E. Narevicius, *Nature Physics* **13**, 35 (2017).
- [8] H. Yang, D.-C. Zhang, L. Liu, Y.-X. Liu, J. Nan, B. Zhao, and J.-W. Pan, *Science* **363**, 261 (2019).
- [9] T. de Jongh, M. Besemer, Q. Shuai, T. Karman, A. van der Avoird, G. C. Groenenboom, and S. Y. van de Meerakker, *Science* **368**, 626 (2020).
- [10] Y. Xie, H. Zhao, Y. Wang, Y. Huang, T. Wang, X. Xu, C. Xiao, Z. Sun, D. H. Zhang, and X. Yang, *Science* **368**, 767 (2020).
- [11] S. D. Gordon, J. J. Omiste, J. Zou, S. Tanteri, P. Brumer, and A. Osterwalder, *Nature Chemistry* **10**, 1190 (2018).
- [12] P. Puri, M. Mills, C. Schneider, I. Simbotin, J. A. Montgomery, R. Côté, A. G. Suits, and E. R. Hudson, *Science* **357**, 1370 (2017).
- [13] S. Ospelkaus, K.-K. Ni, D. Wang, M. De Miranda, B. Neyenhuis, G. Quéméner, P. Julienne, J. Bohn, D. Jin, and J. Ye, *Science* **327**, 853 (2010).
- [14] K.-K. Ni, S. Ospelkaus, D. Wang, G. Quéméner, B. Neyenhuis, M. De Miranda, J. Bohn, J. Ye, and D. Jin, *Nature* **464**, 1324 (2010).
- [15] F. H. Hall and S. Willitsch, *Physical Review Letters* **109**, 233202 (2012).
- [16] W. E. Perreault, N. Mukherjee, and R. N. Zare, *Science* **358**, 356 (2017).
- [17] M. Guo, X. Ye, J. He, M. L. González-Martínez, R. Vexiau, G. Quéméner, and D. Wang, *Physical Review X* **8**, 041044 (2018).
- [18] J. L. Bohn, A. M. Rey, and J. Ye, *Science* **357**, 1002 (2017).
- [19] M. T. Bell and T. P. Softley, *Molecular Physics* **107**, 99 (2009).
- [20] R. D. Levine, *Molecular Reaction Dynamics* (Cambridge University Press, 2009).
- [21] M. Quack, *Molecular Physics* **34**, 477 (1977).
- [22] T. Oka, *Journal of Molecular Spectroscopy* **228**, 635 (2004).
- [23] D. Uy, M. Cordonnier, and T. Oka, *Physical Review Letters* **78**, 3844 (1997).
- [24] M. Cordonnier, D. Uy, R. Dickson, K. Kerr, Y. Zhang, and T. Oka, *The Journal of Chemical Physics* **113**, 3181 (2000).
- [25] A. Faure, P. Hily-Blant, R. Le Gal, C. Rist, and G. P. Des Forêts, *The Astrophysical Journal Letters* **770**, L2 (2013).
- [26] T. Momose, M. Fushitani, and H. Hoshina, *International Reviews in Physical Chemistry* **24**, 533 (2005).
- [27] B. Schramm, D. Bamford, and C. B. Moore, *Chemical Physics Letters* **98**, 305 (1983).
- [28] M. Pealat, D. Debarre, J.-M. Marie, J.-P. Taran, A. Tramer, and C. Moore, *Chemical Physics Letters* **98**, 299 (1983).
- [29] A. D. Webb, R. N. Dixon, and M. N. Ashfold, *The Journal of Chemical Physics* **127**, 224307 (2007).
- [30] M. Mayle, G. Quéméner, B. P. Ruzic, and J. L. Bohn, *Physical Review A* **87**, 012709 (2013).
- [31] A. Christianen, T. Karman, and G. C. Groenenboom, *Physical Review A* **100**, 032708 (2019).
- [32] Y. Liu, M.-G. Hu, M. A. Nichols, D. D. Grimes, T. Karman, H. Guo, and K.-K. Ni, arXiv:2002.05140 (2020).
- [33] P. W. Atkins and R. S. Friedman, *Molecular Quantum Mechanics* (Oxford University Press, 2011).
- [34] Y. Liu, D. D. Grimes, M.-G. Hu, and K.-K. Ni, *Physical Chemistry Chemical Physics* **22**, 4861 (2020).

- [35] S. Ospelkaus, K.-K. Ni, G. Quéméner, B. Neyenhuis, D. Wang, M. De Miranda, J. Bohn, J. Ye, and D. Jin, *Physical Review Letters* **104**, 030402 (2010).
- [36] J. Aldegunde, B. A. Rivington, P. S. Żuchowski, and J. M. Hutson, *Physical Review A* **78**, 033434 (2008).
- [37] M.-G. Hu, Y. Liu, D. Grimes, Y.-W. Lin, A. Gheorghie, R. Vexiau, N. Bouloufa-Maafa, O. Dulieu, T. Rosenband, and K.-K. Ni, *Science* **366**, 1111 (2019).
- [38] K. Aikawa, D. Akamatsu, M. Hayashi, K. Oasa, J. Kobayashi, P. Naidon, T. Kishimoto, M. Ueda, and S. Inouye, *Physical Review Letters* **105**, 203001 (2010).
- [39] J. Banerjee, D. Rahmlow, R. Carollo, M. Bellos, E. E. Eyler, P. L. Gould, and W. C. Stwalley, *Physical Review A* **86**, 053428 (2012).
- [40] S. Falke, I. Sherstov, E. Tiemann, and C. Lisdat, *The Journal of Chemical Physics* **125**, 224303 (2006).
- [41] F. Engelke, H. Hage, and U. Schühle, *Chemical Physics Letters* **106**, 535 (1984).
- [42] J. Y. Seto, R. J. Le Roy, J. Verges, and C. Amiot, *The Journal of Chemical Physics* **113**, 3067 (2000).
- [43] C. Caldwell, F. Engelke, and H. Hage, *Chemical Physics* **54**, 21 (1980).
- [44] C. Amiot and J. Vergès, *Chemical Physics Letters* **274**, 91 (1997).
- [45] D. Yang, J. Zuo, J. Huang, X. Hu, R. Dawes, D. Xie, and H. Guo, *The Journal of Physical Chemistry Letters* **11**, 2605 (2020).
- [46] J. W. Park, Z. Z. Yan, H. Loh, S. A. Will, and M. W. Zwierlein, *Science* **357**, 372 (2017).
- [47] M. Guo, X. Ye, J. He, G. Quéméner, and D. Wang, *Physical Review A* **97**, 020501 (2018).
- [48] P. D. Gregory, J. Aldegunde, J. M. Hutson, and S. L. Cornish, *Physical Review A* **94**, 041403 (2016).
- [49] J. Gong, M. Shapiro, and P. Brumer, *The Journal of Chemical Physics* **118**, 2626 (2003).
- [50] J. Li and S. Kais, *Science Advances* **5**, eaax5283 (2019).
- [51] P. F. Bernath, *Spectra of Atoms and Molecules* (Oxford University Press, 2016).
- [52] S. Lemont, R. Giniger, and G. Flynn, *The Journal of Chemical Physics* **66**, 4509 (1977).
- [53] J. M. Brown and A. Carrington, *Rotational Spectroscopy of Diatomic Molecules* (Cambridge University Press, 2003).
- [54] B. Neyenhuis, B. Yan, S. A. Moses, J. P. Covey, A. Chotia, A. Petrov, S. Kotochigova, J. Ye, and D. S. Jin, *Physical Review Letters* **109**, 230403 (2012).
- [55] K.-K. Ni, *A Quantum Gas of Polar Molecules*, Ph.D. thesis, University of Colorado - Boulder (2009).

Supplementary Material

S1. 1+1' REMPI SPECTROSCOPY

Our REMPI scheme for the state-selective detections of K_2 (Rb_2) utilizes two lasers: a continuous-wave external cavity diode laser operating at 648 (674) nm, and a pulsed Nd:YVO₄ laser with a frequency-doubled output wavelength of 532 nm and a pulse duration of ~ 10 ns. During an experiment, temporally-overlapping light pulses derived from these lasers are repeatedly applied to ionize reaction products. The duration of the 648 (674) nm pulse is controlled by an acoustic-optical modulator (AOM) to be ~ 40 ns, and the relative delay between the two pulses is scanned to maximize the resulting ion signals. The optical power in the 648 and 674 nm beams is 8 and 15 mW, respectively, sufficient to saturate the

targeted transitions. The pulse energy (optical power) of the 532 nm laser is set to be 50 μJ (350 mW), resulting in the ionization of $> 80\%$ of the electronically-excited molecules. The frequencies of the diode lasers are stabilized to an accuracy of 25 MHz through locking to a laser wavelength meter (Bristol 771A).

To avoid excitation of the reactant KRb molecules by the REMPI lasers, we generate dark spots in the centers of the beams using the optical setup illustrated in Fig. S1. The 648/674 nm and 532 nm beams are first combined on a dichroic mirror, and are then sent through a dark mask (Thorlabs R1DF100). The mask is located in the object plane of an achromatic lens ($f = 300$ mm), and is projected onto the image plane coinciding with the molecular cloud location, resulting in the beam profiles shown in the insets. The dark spot size is chosen based on the KRb cloud size, which is up to 80 μm (4σ width) in its longest direction. The length of the dark region along the direction of propagation is approximately 7 mm on either side of the image plane (defined as when the optical intensity inside the dark spot increases to half of the maximal value measured in the image plane).

For $^{40}\text{K}_2$, the bound-to-bound transition lines we target are from the $X^1\Sigma_g^+(v = 0, N) \rightarrow B^1\Pi_u(v' = 1, N')$ vibronic band. The transition dipole moment for these lines is calculated to be $(1.6 e \cdot a_0) \sqrt{S_N^{P,Q,R}}$. Here, e is the electron charge, a_0 is the Bohr radius, and $S_N^{P,Q,R}$ is the Hönl-London factor which takes different forms for P , Q , and R branch rotational transitions. For $\Sigma \rightarrow \Pi$ electronic transitions, they are given by $S_N^P = \frac{N-1}{2N+1}$, $S_N^Q = 1$, and $S_N^R = \frac{N+2}{2N+1}$ [51]. We calculate the linewidth (lifetime) of the excited state to be 14.5 MHz (11 ns), close to the measured value of 13 MHz (12.2 ns) reported in Ref. [52]. An additional contribution to the experimentally measured linewidth is Doppler broadening arising from the large translational energy of K_2 products. For K_2 molecules moving at the maximum velocity allowed by the reaction exothermicity, the Doppler contribution to the linewidth is $\sigma_D \sim 40$ MHz. The REMPI spectroscopy in this work requires knowing transition frequencies better than 0.001 cm^{-1} (or 30 MHz), which is not available from the literature. To identify them, our initial search of the transition lines is guided by frequencies that are calculated using molecular potentials from Ref. [40, 41].

For $^{87}\text{Rb}_2$, the bound-to-bound transition lines we target are from the $X^1\Sigma_g^+(v = 0, N) \rightarrow B^1\Pi_u(v' = 4, N')$ vibronic band. We calculate the transition dipole moment to be $(1.4 e \cdot a_0) \sqrt{S_N^{P,Q,R}}$, and the natural linewidth (lifetime) of the excited state to be 13.9 MHz (11 ns). For Rb_2 molecules moving at the maximum velocity, the Doppler contribution to the linewidth is $\sigma_D \sim 30$ MHz. Our initial search of the transition lines is guided

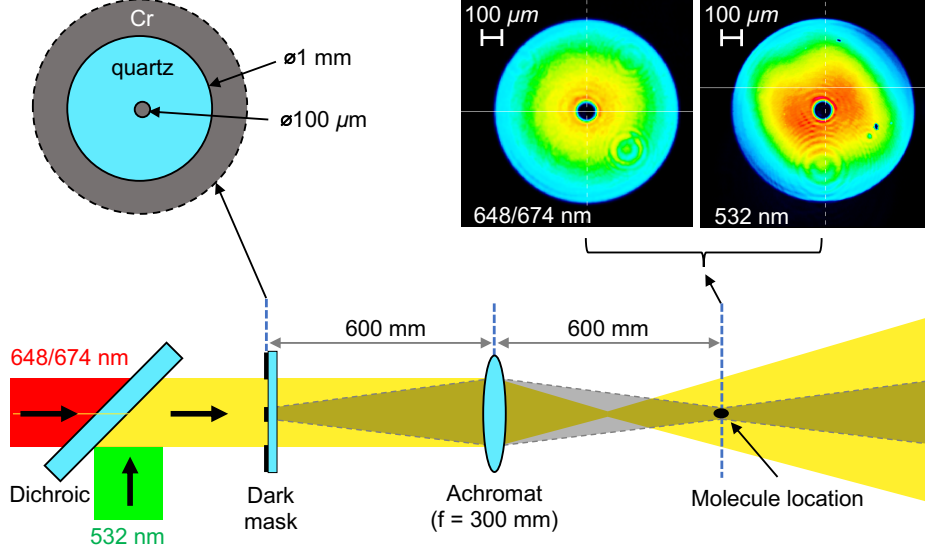


FIG. S1. **The optical setup for generating the REMPI beams.** The 648/674 nm and 532 nm lasers are combined on a dichroic mirror, and are then sent through a dark mask (Thorlabs R1DF100) and an achromatic lens ($f = 300$ mm). The resulting beam profiles in the image plane have a 1 mm outer diameter and a $100 \mu\text{m}$ inner diameter.

by frequencies that are calculated using molecular potentials from Ref. [42–44].

S2. STATE-DECOMPOSITION CALCULATION FOR REACTANT MOLECULES

To obtain the coefficients α , β , and γ of the state-decomposition given in Eq. (2) of the main text, we diagonalize the molecular Hamiltonian for the $^{40}\text{K}^{87}\text{Rb}$ reactants using the basis of uncoupled hyperfine states. If we include the rotational degrees of freedom, we can label these basis states by $|N, m_N, i_{\text{K}}, m_i^{\text{K}}, i_{\text{Rb}}, m_i^{\text{Rb}}\rangle$, where N represents the rotational angular momentum quantum number, m_N is its projection onto the z -axis, $i_{\text{K,Rb}}$ are the nuclear spins of the K and Rb atoms, and $m_i^{\text{K,Rb}}$ are the corresponding projections onto the z -axis. The direction of the z -axis here is defined by an externally applied magnetic field. In the electronic ground state, $X^1\Sigma^+$, as well as the vibrational ground state, the molecular Hamiltonian in the presence of external electric and magnetic fields can be expressed as [36, 53],

$$H = H_{\text{rot}} + H_{\text{HF}} + H_{\text{S}} + H_{\text{Z}}. \quad (\text{S1})$$

Here,

$$H_{\text{rot}} = B_{\text{rot}} \mathbf{N}^2, \quad (\text{S2})$$

$$H_{\text{HF}} = -e(\nabla\mathbf{E})_{\text{K}} \cdot \mathbf{Q}_{\text{K}} - e(\nabla\mathbf{E})_{\text{Rb}} \cdot \mathbf{Q}_{\text{Rb}} + c_{\text{K}} \mathbf{N} \cdot \mathbf{I}_{\text{K}} + c_{\text{Rb}} \mathbf{N} \cdot \mathbf{I}_{\text{Rb}} + c_4 \mathbf{I}_{\text{K}} \cdot \mathbf{I}_{\text{Rb}}, \quad (\text{S3})$$

$$H_S = -\boldsymbol{\mu} \cdot \mathbf{E}, \quad (\text{S4})$$

$$H_Z = -g_r \mu_N \mathbf{N} \cdot \mathbf{B} - g_K \mu_N (1 - \sigma_K) \mathbf{I}_K \cdot \mathbf{B} - g_{\text{Rb}} \mu_N (1 - \sigma_{\text{Rb}}) \mathbf{I}_{\text{Rb}} \cdot \mathbf{B}, \quad (\text{S5})$$

where \mathbf{N} is the rotational angular momentum operator, $\mathbf{I}_{\text{K,Rb}}$ are the nuclear spin operators for the K and Rb nuclei, respectively, $(\nabla \mathbf{E})_{\text{K,Rb}}$ are the intramolecular electric field gradients at the K and Rb nuclei, respectively, $e\mathbf{Q}_{\text{K,Rb}}$ are the nuclear electric quadrupole moment operators for K and Rb, respectively, $\boldsymbol{\mu}$ is the molecular dipole moment, \mathbf{E} is the external electric field, \mathbf{B} is the external magnetic field, and e is the charge of the electron.

In this molecular Hamiltonian, Eq. (S2) denotes the rotational contribution to the energy, with corresponding rotational constant $B_{\text{rot}}/h = 1.1139514 \text{ GHz}$ [35, 54]. Eq. (S3) represents the hyperfine energy, where $-e(\nabla \mathbf{E})_i \cdot \mathbf{Q}_i$ describes the interaction between the intramolecular electric field gradient at nucleus i and the corresponding nuclear electric quadrupole moment, which is characterized by the electric quadrupole coupling constants $(eqQ)_K/h = 0.452 \text{ MHz}$ and $(eqQ)_{\text{Rb}}/h = -1.308 \text{ MHz}$ [54]. The remaining three terms in Eq. (S3) describe the interactions of the individual nuclear spins with the magnetic field associated with the rotation of the molecule, where the corresponding coupling constants are given by $c_K/h = -24.1 \text{ Hz}$ and $c_{\text{Rb}}/h = 420.1 \text{ Hz}$ [36], as well as the scalar nuclear spin-spin interaction, with an associated coupling constant $c_4/h = -2030.4 \text{ Hz}$ [36]. The Stark Hamiltonian given by Eq. (S4) describes the interaction between the permanent electric dipole moment of KRb, $\mu = 0.574 \text{ Debye}$ [55], and an external electric field. The Zeeman contribution to the energy (Eq. (S5)), on the other hand, consists of three separate terms: the interaction between the external magnetic field and the magnetic moment arising from molecular rotation, with a corresponding rotational g -factor of $g_r = 0.014$ [36], and the interactions between the magnetic moments of the individual nuclei, whose g -factors are given by $g_K = -0.324$ and $g_{\text{Rb}} = 1.834$ [36], and the external magnetic field. The remaining parameters in Eq. (S5), μ_N and $\sigma_{\text{K,Rb}}$, represent the nuclear magneton and the nuclear shielding constants, respectively. For the K and Rb nuclei, the nuclear shielding constants are $\sigma_K = 1321 \text{ ppm}$ and $\sigma_{\text{Rb}} = 3469 \text{ ppm}$ [36].

For the reactant state-decomposition calculations shown in the main text (Fig. 4(a)), we include rotational states up to $N_{\text{max}} = 1$ when diagonalizing this Hamiltonian in the basis of uncoupled hyperfine states, $|N, m_N, i_K, m_i^K, i_{\text{Rb}}, m_i^{\text{Rb}}\rangle$, where $i_K = 4$ and $i_{\text{Rb}} = 3/2$. We also make use of the fact that the ground-state molecules are initially prepared at zero electric field and at a high magnetic field, $B \approx 544 \text{ G}$, where the un-

coupled basis states are a good representation of the eigenstates of the molecular Hamiltonian (Eq. (S1)). In this configuration, the KRb molecules are produced in their rotational, vibrational, and electronic ground state, and in the hyperfine state $|\psi_{\text{KRb}}^i\rangle \equiv |N=0, m_N=0, i_K=4, m_i^K=-4, i_{\text{Rb}}=3/2, m_i^{\text{Rb}}=1/2\rangle$ [34]. This corresponds to the situation where $\alpha \approx 1$ and $\beta = \gamma \approx 0$ in Eq. (2) of the main text. As the electric and magnetic fields are changed adiabatically following the initial preparation of the reactant molecules, we obtain the coefficients α , β , and γ by diagonalizing the molecular Hamiltonian (Eq. (S1)) at the desired values of the electric and magnetic fields, and selecting the eigenstate which is adiabatically connected to the initial hyperfine state, $|\psi_{\text{KRb}}^i\rangle$. The coefficients of the expansion of this eigenstate in terms of the uncoupled basis states are then α , β , and γ . For the calculations shown in Fig. 4(a) of the main text, we set $E = 0$ for simplicity, as the small electric field used in the experiment, $E = 18 \text{ V/cm}$, has a negligible effect on the state-decomposition, and we numerically calculate α , β , and γ as a function of the magnetic field.

S3. SELECTION RULES FOR NUCLEAR SPIN CONSERVATION IN ULTRACOLD REACTIONS

Selection rules in chemical reactions arise when the S -matrix is diagonalizable in a basis made up of the eigenstates of some conserved quantity, also known as a collision constant [21]. Due to their weak couplings to other degrees of freedom, nuclear spins of molecules may be conserved in chemical reactions [22] and so their eigenstates may be used to derive one such selection rule. For ultracold reactions of bi-alkali molecules of the form, $\text{AB} + \text{AB} \rightarrow \text{A}_2 + \text{B}_2$, the nuclear spin states of the heteronuclear reactants can be described in the uncoupled basis, $\{|i_{\text{A1}}, i_{\text{B1}}, m_{\text{A1}}, m_{\text{B1}}\rangle \otimes |i_{\text{A2}}, i_{\text{B2}}, m_{\text{A2}}, m_{\text{B2}}\rangle\}$, while those of the homonuclear products are more naturally expressed in the coupled basis, $\{|I_{\text{A}_2}, M_{\text{A}_2}; i_{\text{A1}}, i_{\text{A2}}\rangle \otimes |I_{\text{B}_2}, M_{\text{B}_2}; i_{\text{B1}}, i_{\text{B2}}\rangle\}$, in which the states obey the exchange symmetry of identical nuclei. Here, A1 (A2) and B1 (B2) denote atomic nuclei from the 1st (2nd) AB molecules in the reaction. The total spin is defined as $\mathbf{I}_{\text{A}_2(\text{or B}_2)} = \mathbf{i}_{\text{A1}(\text{or B1})} + \mathbf{i}_{\text{A2}(\text{or B2})}$ and its projection is $M_{\text{A}_2(\text{or B}_2)} = m_{\text{A1}(\text{or B1})} + m_{\text{A2}(\text{or B2})}$. The coupled basis state $|I, M; i_1, i_2\rangle$ is symmetric under interchange of particles 1 and 2 if $i_1 + i_2 - I$ is even, and antisymmetric if $i_1 + i_2 - I$ is odd.

To obtain the probabilities for scattering into different channels, or product states, we can transform the reactant nuclear spin state from the uncoupled basis into the coupled basis. The coefficients of the reactant state in the coupled basis then provide the desired information

regarding the branching into the different reaction channels. This basis transformation can be performed using the general formula for the addition of angular momentum,

$$|i_1, i_2, m_1, m_2\rangle = \sum_{I=|i_1-i_2|}^{i_1+i_2} \langle I, M; i_1, i_2 | i_1, i_2, m_1, m_2 \rangle |I, M; i_1, i_2\rangle, \quad (\text{S6})$$

where $M = m_1 + m_2$ and $\langle I, M; i_1, i_2 | i_1, i_2, m_1, m_2 \rangle$ are the Clebsch-Gordan (CG) coefficients. Take the reactant state

$$\psi_{\text{KRb}} = \alpha \left| 4, \frac{3}{2}, -4, \frac{1}{2} \right\rangle + \beta \left| 4, \frac{3}{2}, -3, -\frac{1}{2} \right\rangle + \gamma \left| 4, \frac{3}{2}, -2, -\frac{3}{2} \right\rangle, \quad (\text{S7})$$

for example. Assuming that nuclear spins are spectators during the reaction, we can write

the reactant nuclear spin state,

$$\begin{aligned}
\psi_{\text{KRb}} \otimes \psi_{\text{KRb}} &= \alpha^2 \left| 4, \frac{3}{2}, -4, \frac{1}{2} \right\rangle \otimes \left| 4, \frac{3}{2}, -4, \frac{1}{2} \right\rangle + \beta^2 \left| 4, \frac{3}{2}, -3, -\frac{1}{2} \right\rangle \otimes \left| 4, \frac{3}{2}, -3, -\frac{1}{2} \right\rangle \\
&\quad + \gamma^2 \left| 4, \frac{3}{2}, -2, -\frac{3}{2} \right\rangle \otimes \left| 4, \frac{3}{2}, -2, -\frac{3}{2} \right\rangle + \{\dots\} \\
&= \alpha^2 |4, 4, -4, -4\rangle \otimes \left| \frac{3}{2}, \frac{3}{2}, \frac{1}{2}, \frac{1}{2} \right\rangle + \beta^2 |4, 4, -3, -3\rangle \otimes \left| \frac{3}{2}, \frac{3}{2}, -\frac{1}{2}, -\frac{1}{2} \right\rangle \\
&\quad + \gamma^2 |4, 4, -2, -2\rangle \otimes \left| \frac{3}{2}, \frac{3}{2}, -\frac{3}{2}, -\frac{3}{2} \right\rangle + \{\dots\} \\
&= \alpha^2 |8, -8\rangle \otimes \left(\sqrt{\frac{3}{5}} |3, 1\rangle - \sqrt{\frac{2}{5}} |1, 1\rangle \right) \tag{S8}
\end{aligned}$$

$$+ \beta^2 \left(-\sqrt{\frac{7}{15}} |6, -6\rangle + \sqrt{\frac{8}{15}} |8, -6\rangle \right) \otimes \left(\sqrt{\frac{3}{5}} |3, -1\rangle - \sqrt{\frac{2}{5}} |1, -1\rangle \right) \tag{S9}$$

$$+ \gamma^2 \left(\sqrt{\frac{45}{143}} |4, -4\rangle - \sqrt{\frac{14}{55}} |6, -4\rangle + \sqrt{\frac{28}{65}} |8, -4\rangle \right) \otimes |3, -3\rangle \tag{S10}$$

$$+ \alpha\beta |8, -7\rangle \otimes \left(\sqrt{\frac{9}{10}} |3, 0\rangle - \sqrt{\frac{1}{10}} |1, 0\rangle \right) \tag{S11}$$

$$+ \alpha\gamma \left(\sqrt{\frac{8}{15}} |6, -6\rangle + \sqrt{\frac{7}{15}} |8, -6\rangle \right) \otimes \left(\sqrt{\frac{3}{5}} |1, -1\rangle + \sqrt{\frac{2}{5}} |3, -1\rangle \right) \tag{S12}$$

$$+ \beta\gamma \left(\frac{2}{\sqrt{5}} |8, -5\rangle - \frac{1}{\sqrt{5}} |6, -5\rangle \right) \otimes |3, -2\rangle \tag{S13}$$

$$+ \alpha\beta |7, -7\rangle \otimes \sqrt{\frac{1}{2}} (|0, 0\rangle - |2, 0\rangle) \tag{S14}$$

$$- \alpha\gamma |7, -6\rangle \otimes |2, -1\rangle \tag{S15}$$

$$+ \beta\gamma \left(\sqrt{\frac{9}{13}} |5, -5\rangle - \sqrt{\frac{4}{13}} |7, -5\rangle \right) \otimes |2, -2\rangle, \tag{S16}$$

where we have used Eq. (S6) from the step two to the step three, and $\{\dots\}$ represents all additional terms. The last step gives the reactant state in the coupled basis, where we omit values of i_K and i_{Rb} for convenience. Each of the resulting tensor product states in Eqs. (S8-

(S16) corresponds to a possible scattered channel. Among them, the terms in Eqs. (S14-S16) are antisymmetric under the exchange of identical nuclei, while all others are symmetric. Therefore the total probability for scattering into an antisymmetric nuclear spin state of the products is given by, $P_A = |\alpha\beta|^2 + |\alpha\gamma|^2 + |\beta\gamma|^2$, whereas that for scattering into a symmetric state is $P_S = 1 - P_A$. Furthermore, based on the exchange symmetry of identical nuclei, the populations of even (odd) rotational states of the products are thus proportional to P_S (P_A) when the nuclei are bosonic, and are proportional to P_A (P_S) when the nuclei are fermionic.

While this result was derived for a specific input state Eq. (S7), the methodology does not depend on the particular form of this state, so that the formulae for P_A and P_S can be generalized to account for any initial states of the reactants. Additionally, as far as the summed probabilities are concerned, it is not strictly necessary to consider the CG coefficients of the dressed product states in the presence of a magnetic field. Instead, it is sufficient, for the purposes of this work, to consider only the CG coefficients of the bare states in the absence of a field. However, for a state-to-state measurement which resolves individual nuclear spin states, it is, strictly speaking, necessary to consider the CG coefficients of the dressed states. This will be reported in another work.